Global DEM Product Generation by Correcting ASTER GDEM Elevation with ICESat-2 Altimeter Data

Binbin Li[1,2,3,4], Huan Xie[1,5], Shijie Liu[1], Zhen Ye[1], Zhonghua Hong[6], Qihao Weng[2,3,4], Yuan Sun[1], Qi Xu[1], Xiaohua Tong[1]

[1]College of Surveying and Geo-informatics, and Shanghai Key Laboratory for Planetary Mapping and Remote Sensing for Deep Space Exploration, Tongji University, Shanghai 200092, China
[2]JC STEM Lab of Earth Observations, Department of Land Surveying and Geo-Informatics, The Hong Kong Polytechnic University, Hung Hom, Hong Kong 999077, China
[3]Research Centre for Artificial Intelligence in Geomatics, The Hong Kong Polytechnic University, Hung Hom, Hong Kong 999077, China
[4]Research Institute for Land and Space, The Hong Kong Polytechnic University, Hung Hom, Hong Kong 999077, China
[5]College of Information Technology, Shanghai Ocean University, Shanghai 201306, China
[6]Shanghai Institute of Intelligent Science and Technology, Tongji University, Shanghai 200092, China

Correspondence to: Huan Xie (huanxie@tongji.edu.cn)

Abstract. Advancements in scientific inquiry and practical applications have put forward a higher demand for the accuracy of global digital elevation models (GDEMs), especially for GDEMs whose main data source is optical imagery. To address this challenge, integrating GDEM and satellite laser altimeter data (global coverage and high-accuracy ranging) is one of the important research directions, in addition to the technological enhancement of the main data source. In this paper, we describe the datasets and algorithms used to generate a GDEM product (IC2-GDEM) by correcting ASTER GDEM elevation data with ICESat-2 altimeter data. The algorithm scheme presents the details of the strategies used for the various challenges, such as the processing of DEM boundaries, the fusion of the different data, the geographical layout of the satellite laser altimeter data, etc. We used a high-accuracy global elevation control point dataset and multiple high-accuracy local DEMs as the validation data for a comprehensive assessment at a global scale. The results from the validation comparison present that the elevation accuracy of IC2-GDEM is evidently superior to that of the ASTER GDEM product. The root-mean-square error (RMSE) reduction ratio of the corrected GDEM elevation is between 16% and 82%, and the average reduction ratio is about 47%. From the analysis of the different topographies and land covers, it was also found that this error reduction is effective even in areas with high topographic relief (>15°) and high vegetation cover (>60%). ASTER GDEM has been in use for more than a decade, and many historical datasets and models are based on its elevation data. IC2-GDEM facilitates seamless integration with these historical datasets, which is essential for longitudinal studies examining long-term environmental change, land use dynamics, and climate impacts. Meanwhile, IC2-GDEM can serve as a new complementary data source to existing DEMs (Copernicus DEM, etc.) mainly sourced from synthetic aperture radar (SAR) observation. By cross-validating qualities, filling data gaps, conducting multi-scale analyses, etc., it can lead to more reliable and comprehensive scientific discoveries, thereby improving the overall quality and reliability of earth science research. IC2-GDEM product is openly released via https://doi.org/10.11888/RemoteSen.tpdc.301229 (Xie et al., 2024).

1 Introduction

High-quality digital elevation model (DEM) data are of great significance for the field of Earth science research and scientific applications, including hydrological modeling, climate change research, natural hazard assessment, and ecosystem management. For example, high-quality DEMs can improve the accuracy of watershed delineation and flood risk assessment, promoting effective water resources management and disaster preparedness (Ao et al., 2024). In climate change research, high-quality DEMs are vital for the modeling of glacier dynamics and the sea level rise impact, thereby improving predictive accuracy and informing mitigation strategies (Fan et al., 2022; Cook et al., 2012).

Airborne LiDAR/radar and high-resolution imaging systems can produce DEMs with a centimeter to sub-meter accuracy, but this kind of DEM is costly to derive. As a result, such DEMs are not extensively accessible at a global scale (Pham et al., 2018). Laser altimeters carried on satellite platforms (Schutz et al., 2005; Xie et al., 2021; Dubayah et al., 2020; Martino et al., 2019; Tang et al., 2020) such as ICESat, ICESat-2, etc., can provide accurate elevation information around the world, and their elevation information is freely available. The accuracy of the elevation information can attain a meter, sub-meter, or even centimeter level after data refinement (Li et al., 2023c; Zhu et al., 2022; Neuenschwander et al., 2020; Fernandez-Diaz et al., 2022; Li et al., 2021). Previous studies have refined ICESat/ICESat-2 altimeter data in polar regions to produce and release polar DEM products (Shen et al., 2022; Fan et al., 2021). However, at present, it is still difficult to use satellite laser altimeter data to generate DEMs with a medium resolution at a global scale, due to the limitation of the spacing between ground tracks (Magruder et al., 2021). At a global scale, analysis of the spatial elevation at a medium resolution still relies on DEMs derived from other satellite technologies (optical imaging, synthetic aperture radar (SAR), etc.), but the accuracy of this kind of DEM data is lower, at multiple meters or even more than 10 m (Meadows et al., 2024; Al-Areeq et al., 2023; Yue et al., 2017; Del Rosario González-Moradas et al., 2023; Hawker et al., 2019). This data characteristic is challenged by the related scientific applications with a requirement for higher and higher elevation accuracy. Therefore, improving the accuracy of this kind of DEM data has been widely focused on and studied by many scholars. In addition to technological improvement, integrating DEM with satellite laser altimeter data is one of the important research directions. Scholars have also provided important guidance and reference to this field by using linear fitting, machine/deep learning, and other methods (Li et al., 2023a; Magruder et al., 2021; Hawker et al., 2022).

Free global DEMs (GDEMs) with a medium resolution include the Advanced Spaceborne Thermal Emission and Reflection Radiometer global digital elevation model (ASTER GDEM) (Abrams et al., 2015), the Shuttle Radar Topography Mission (SRTM) DEMs (Farr et al., 2007), and the Copernicus GLO-30 DEM (Fahrland et al., 2022), etc. The data source of these DEMs can divided into two main kinds: 1) optical imaging (for the ASTER GDEM); and 2) SAR (for the SRTM DEMs and Copernicus GLO-30 DEM). Owing to the noise and anomalies resulting from the limitations inherent in optical imaging, the elevation quality of the ASTER GDEM is typically deemed to be lower than that of the other GDEMs for which the source is radar data (Meadows et al., 2024; Del Rosario González-Moradas et al., 2023), such as the SRTM DEMs, Copernicus GLO-30 DEM, etc. In addition, a survey of some studies showed that the role of GDEMs for which the main source is optical

imaging has not been completely replaced. For example, the ASTER GDEM elevation shows a higher quality than the SRTM elevation in some mountainous areas (Li et al., 2013; Yue et al., 2017), and also shows a better quality than the Copernicus

70   GLO-30 DEM in some areas with steep topography (Del Rosario González-Moradas et al., 2023) or high vegetation cover (Okolie et al., 2024; Huang and Yu, 2024). Furthermore, some studies (Pham et al., 2018; Yamazaki et al., 2017; Crippen et al., 2016; Franks et al., 2020; Okolie and Smit, 2022) have also reported that diversified choices and complementary use strategies for GDEMs are still favored by many scholars and users. For instance, the data sources for the void filling of the Copernicus GLO-30 DEM consist of other DEMs, including the ASTER GDEM, SRTM DEMs, and several national DEMs

75   (Del Rosario González-Moradas et al., 2023). It is therefore of great significance to obtain more accurate ASTER GDEM elevation products to promote the development of this field. Researchers can use the enhanced ASTER GDEM in conjunction with other DEM products to cross-validate qualities, fill data gaps, and conduct multi-scale analyses. This complementary use of multiple DEMs can lead to more reliable and comprehensive scientific discoveries, thereby improving the overall quality and reliability of geoscience research. However, few previous studies have focused on integrating ASTER GDEM and satellite

80   laser altimeter data to generate and release a new enhanced ASTER GDEM product at a global scale.

In this study, given this issue, we collected multiple sets of data with a global coverage, including ICESat-2 altimeter data, a global land-cover product, a global vegetation index product, and ASTER GDEM Version 3 data (the most up-to-date version) to correct the ASTER GDEM elevation and build a corresponding corrected product for further exploring and enhancing the applicability of the GDEMs whose main data source is optical imagery. Taking into account the particularity of polar areas,

85   namely the high variability of ice sheets and ice flow rates, etc., the corrected product covers the global land areas but not polar areas. Moreover, in our previous study, we presented a high-accuracy ICESat-2 elevation correction method (Li et al., 2021) and a DEM elevation correction model (Li et al., 2023a). In this study, based on these models, we further optimized and designed an automatic processing scheme for correcting ASTER GDEM elevation. The scheme introduces detailed strategies for the various challenges, such as the processing of DEM boundaries, the fusion of different data, the geographical layout of

90   the ICESat-2 altimeter data, etc. The details of the scheme will provide a meaningful reference for related fields. Meanwhile, a high-accuracy global control point dataset and multiple local DEMs (LDEMs) with a high resolution and accuracy were used to validate the accuracy of the original and refined ASTER GDEM, including comparison of the elevation accuracy in areas with different geolocations, topographic relief, and vegetation cover. The related analysis results will provide a beneficial supplement for the accuracy qualification of the latest ASTER GDEM with different geolocations, altitudes, topography,

95   vegetation cover, etc. Moreover, ASTER GDEM has been used for more than a decade, and many historical datasets and models are based on its elevation data. The release of refined ASTER GDEM facilitates seamless integration with historical datasets, which is essential for longitudinal studies examining long-term environmental changes, land use dynamics, and climate impacts.

Throughout the remainder of this paper, we introduce the materials (Section II), present the methodology (Section III), and

100 compare the accuracy of the ASTER GDEM before and after elevation correction (Section IV). Finally, we draw our conclusions in Section V.

2 Materials

2.1 Satellite Laser Altimeter Data

The ICESat-2 satellite embarked on its mission in 2018 (Martino et al., 2019). This satellite operates in a near-polar orbit,
105   skimming the Earth at a low altitude of 496 km, featuring an orbital inclination of 92 degrees, and completing its cycle every
91 days. (Martino et al., 2019; Markus et al., 2017). The satellite (Markus et al., 2017) carries a new type of laser altimeter,
i.e., a photon-counting laser altimeter, which observes global areas with three pairs of laser beams. These characteristics result
in the observations at higher-latitude areas being denser than those at lower-latitude areas. Moreover, compared with previous
altimeters, this altimeter only requires low laser transmission energy to observe a profile with a smaller laser footprint along
110   the ground track.

The ATL08 product (Neuenschwander and Pitts, 2019) was used in this study, spanning a survey period from 2018 to 2022.

2.2. GDEM with a Medium Resolution

The ASTER GDEM Version 3 (Abrams et al., 2020) was produced through the utilization of stereo-pair images captured by
the ASTER instrument onboard the Terra satellite. The DEM covers land areas between 83°N and 83°S, offering a spatial
115   resolution of approximately 30 m. The whole DEM is split into over 20,000 files. The geo-boundary of each file is 1° × 1°.
Given the particularity of polar areas, namely the high variability of ice sheets and ice flow rates, and the dense observations
of satellite altimeter data, etc., only the parts of the product within the land areas between 83°N and 60°S (except for polar
areas) were corrected.

2.3. Auxiliary Data

120   A global land-cover product and a global vegetation index product were used to generate the evaluation attribute set for the
GDEM elevation. In this study, the global land-cover product was FROM-GLC10, for which the resolution is about 10 m
(Gong et al., 2019), and the global vegetation index product was GFCC30TC, which has a resolution of about 30 m (Sexton
et al., 2013; García-Álvarez and Lara Hinojosa, 2022). These two data sources were matched with the ASTER GDEM by
resampling.

125   ### 2.4 Validation Data

Two different kinds of validation data were used in this study, according to the type of survey platform (i.e., satellite and
airborne platforms). The first was a high-accuracy global elevation control point dataset (HAGECPD) (Li et al., 2022). The
source of the HAGECPD data is ICESat altimeter data with a survey time between 2003 and 2009. In HAGECPD, the elevation
control points cover the global land area between 83°N and 60°S. The resolution of these elevation control points is more than
130   a hectometer along the ground track, and the distance separating the ground tracks typically measures around ~7 kilometers.
Figure 1 illustrates the elevation control points distributed across a grid of 1° × 1°. The RMSE of these elevation control points

is about 0.5 to 3 m. The second source of validation data was LDEM data from around the world, for which the spatial distribution of the data is depicted in Figure 2. These LDEM data were generated from LiDAR data collected via airborne platform or images captured by unmanned aerial vehicles in conjunction with LiDAR data. Compared with the first type of validation data, these LDEM data have a high resolution and accuracy. The detailed characteristics of the LDEM data are listed in Table 1. These LDEM data were collected according to the following criteria: 1) the data were freely available; 2) the topography and land cover of these data were diverse; 3) the geolocations of these data were diverse around the world.
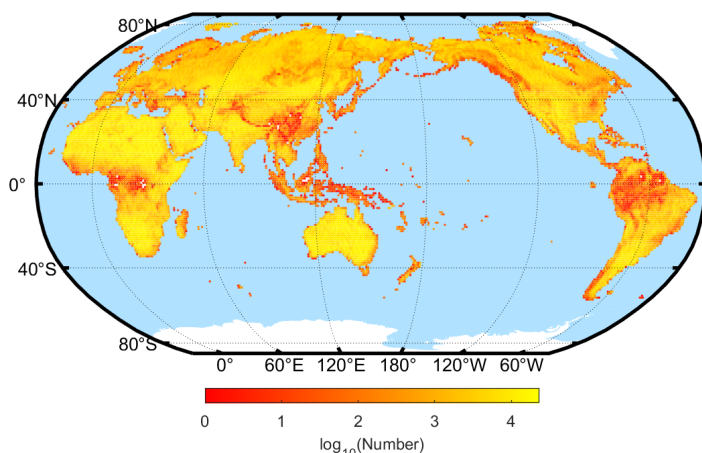
Figure 1: Distribution of the elevation control points at 1° × 1° (redrawn from (Li et al., 2022)).

Compared with the second type of validation data, HAGECPD has a lower data density and accuracy but a global coverage. The HAGECPD data were used to validate the accuracy of the corrected ASTER GDEM with the different geographical locations and altitudes at a global scale. The LDEM data were used to validate the accuracy of the corrected ASTER GDEM with the different topographies and vegetation cover as they have a high data density and accuracy and their areas have diverse topography and vegetation cover.

Table 1 Main data characteristics of the LDEMs with high resolution and accuracy

LDEM	Year	Resolution(m)	Vertical RMSE (cm)
a–e	2001–2016	5	~15
f	2018–2020	1	~10
g	2018	1	~7
h	2016	1	~5
i	2020	0.5	~5

j	2017	0.5	~5
k–n	2014–2015	5	~36 to ~78
o–r	2014–2017		~20 to 44
s	2020	1	~6
t	2020–2021	1	~10
u	2016–2017	1	~10
v	2016–2018	1	~10
w	2020–2022	0.5	~10
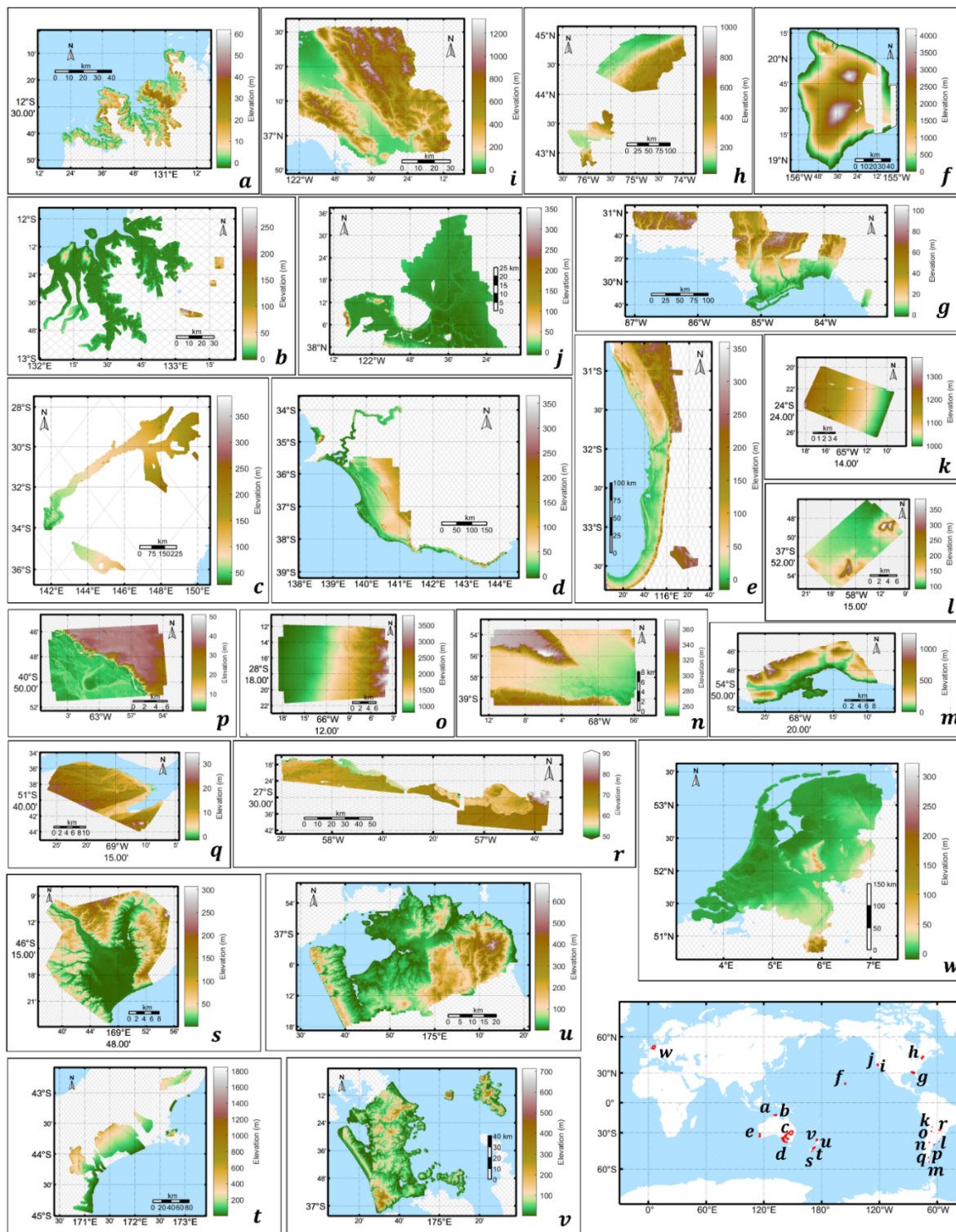
Earth System Science Data Discussions
Figure 2: Distribution of the LDEMs with high resolution and accuracy.

150

3. Methodology

The processing flow for correcting GDEM elevation, as shown in Figure 3, includes four main parts: 1) DEM prepossessing; 2) construction of the elevation evaluation attribute set; 3) generation of the elevation deviation; and 4) DEM elevation correction.
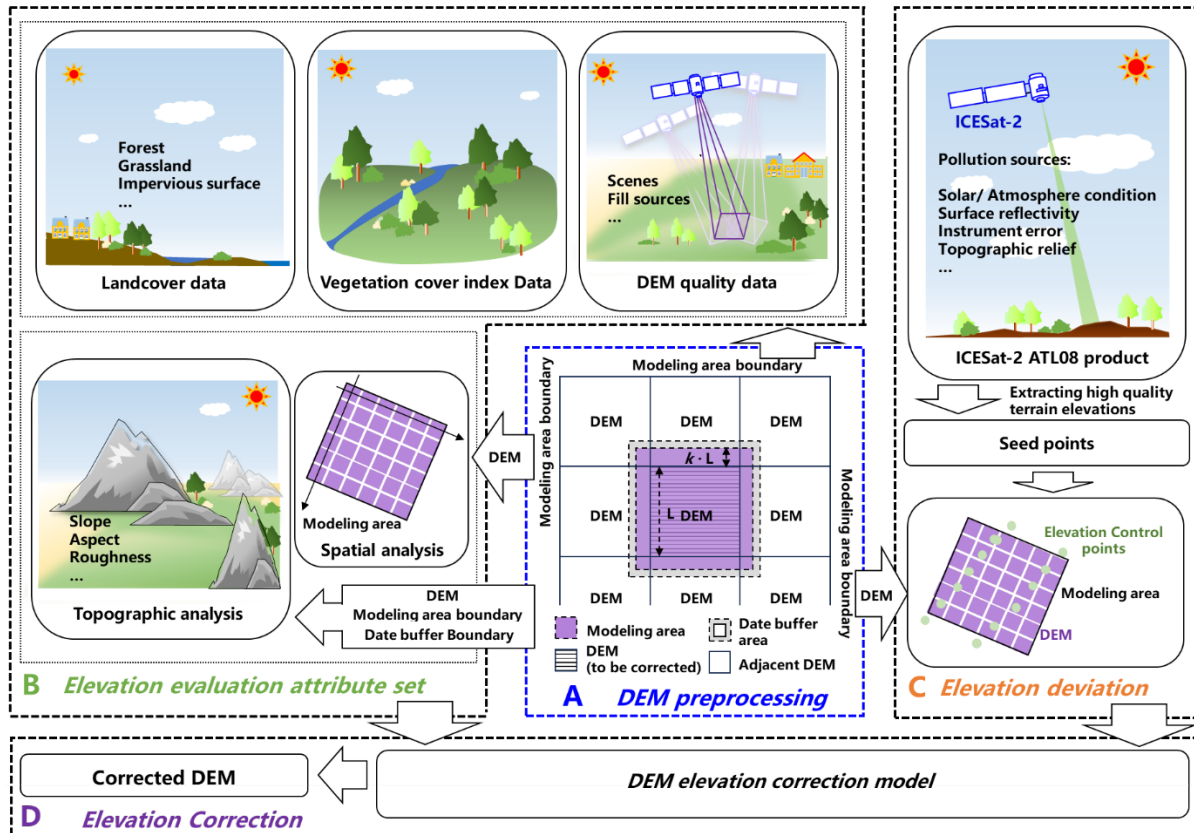
Figure 3: Main flowchart for GDEM correction.

3.1. GDEM Prepossessing

The elevations of the ASTER GDEM were corrected one by one for each $1° \times 1°$ DEM file. In the correction, the following challenges needed to be considered: 1) there can be insufficient ICESat-2 altimeter data in some DEM files, especially in the land margin areas with a low proportion of effective land area, which can reduce the performance of the correction model within these areas; 2) elevation continuity between adjacent DEM elevations should be ensured after correction; and 3) DEM boundary pixels lack enough adjacent information, which can affect the accuracy of the evaluation attribute set of these boundary pixels. To address these challenges, it was necessary to expand the area around the DEM file to be corrected. As shown in part A of Figure 3, the expanded area includes two types: the modeling area and the data buffer area. The modeling

area was used to address challenges 1) and 2), and the data buffer data was used to address challenge 3). The calculations for the modeling and data buffer areas were as follows:

$$\begin{bmatrix} \Phi_m^{max} \\ \Lambda_m^{min} \end{bmatrix} = R_{ref} \cdot \left(\begin{bmatrix} r_{DEM}^{ul} \\ c_{DEM}^{ul} \end{bmatrix} - k \cdot L \right) \tag{1}$$

$$\begin{bmatrix} \Phi_m^{min} \\ \Lambda_m^{max} \end{bmatrix} = R_{ref} \cdot \left(\begin{bmatrix} r_{DEM}^{dr} \\ c_{DEM}^{dr} \end{bmatrix} + k \cdot L \right) \tag{2}$$

$$\begin{bmatrix} \Phi_b^{min} \\ \Lambda_b^{max} \end{bmatrix} = R_{ref} \cdot \left(\begin{bmatrix} r_{DEM}^{dr} \\ c_{DEM}^{dr} \end{bmatrix} - k \cdot L - \Delta L \right) \tag{3}$$

$$\begin{bmatrix} \Phi_b^{min} \\ \Lambda_b^{max} \end{bmatrix} = R_{ref} \cdot \left(\begin{bmatrix} r_{DEM}^{dr} \\ c_{DEM}^{dr} \end{bmatrix} + k \cdot L + \Delta L \right) \tag{4}$$

$$L = \max \left((r_{DEM}^{dr} - r_{DEM}^{ul}), (c_{DEM}^{dr} - c_{DEM}^{ul}) \right) \tag{5}$$

where $[r_{DEM}^{ul}, c_{DEM}^{ul}]^T$ and $[r_{DEM}^{ul}, c_{DEM}^{ul}]^T$ respectively represent the pixel coordinates of the left vertex and bottom right pixel coordinates of the DEM to be corrected; R_{ref} represents the transformation matrix of pixel coordinates to geographic coordinates for the DEM to be corrected, which can be obtained directly from the DEM file; and k and ΔL represent the pixel expansion coefficient and pixel expansion increment, respectively. The initial setting of k was 0.1. ΔL was set to 10, which could ensure that the boundary pixels of the modeling area had sufficient adjacent information.

3.2. Generation of the GDEM Elevation Evaluation Attribute Set

The sources for the attribute set included the ASTER GDEM (elevation and quality data), the land-cover and the vegetation cover data. However, there were inconsistencies in the resolution of these data sources. Before constructing the attribute set, it was necessary to match each ASTER GDEM pixel with the other data based on the criterion of the nearest geographical location.

After matching, each pixel $p_i(\lambda_i, \varphi_i, h_i, q_i, \eta_i, \zeta_i)$ (called an attribute pixel) contained the geographical location (longitude λ_i and latitude φ_i), elevation h_i, elevation quality q_i, vegetation cover index ζ_i, and land-cover category η_i. Then, for each DEM of the ASTER GDEM, the corresponding attribute pixel sets P_b and P_m were extracted according to the boundaries of the modeling and data buffer areas, respectively, as shown in the following formulas:

$$P_b = \bigcup_{i=1}^{N} p_i(\lambda_i \in [\Lambda_b^{min}, \Lambda_b^{max}], \varphi_i \in [\Phi_b^{min}, \Phi_b^{max}]) \tag{6}$$

$$P_m = \bigcup_{i=1}^{N} p_i(\lambda_i \in [\Lambda_m^{min}, \Lambda_m^{max}], \varphi_i \in [\Phi_m^{min}, \Phi_m^{max}]) \tag{7}$$

where N represents the total pixel number of the DEM to be processed and its neighboring DEM. According to the Earth's surface information, P_b^{nw} (P_b within the water-free area) and P_m^{nw} (P_m within the water-free area) were extracted, respectively, as shown in the following formulas:

$$P_b^{nw} = P_b \cap P_{nw} \tag{8}$$

$$P_m^{nw} = P_m \cap P_b^{nw} \tag{9}$$

$$P_{nw} = \bigcup_{i=1}^{N} pi(h_i \neq 0, \eta_i \neq 60, \zeta_i \neq 200) \tag{10}$$

195   where P_{nw} represents the set of attribute pixels within the water-free area of the DEM to be processed and its neighboring DEM. Then, according to our previous study (Li et al., 2023a), the attribute pixels in P_b^{nw} were used to generate the evaluation features for the topography, and those in P_m^{nw} were used to generate the other evaluation features.

3.3. Generation of the GDEM Elevation Deviation

The accuracy of ICESat-2 altimeter data significantly exceeds that of ASTER GDEM data. ICESat-2 altimeter data can be
200   used as the source of the accurate elevation references (i.e., seed points) for the ASTER GDEM to generate the training samples. For the training samples, the seed points can be expected to be of better quality, followed by a more even distribution, and of greater quantity. However, there is a contradiction between these indicators. On a global scale, it was necessary to make comprehensive consideration of these indicators in each DEM area of the ASTER GDEM. For this comprehensive consideration, in our prior study, we presented a method for deriving accurate elevations from ICESat-2 altimeter data with
205   the comprehensive evaluation labels. We then analyzed the performance of each evaluation label, and discussed a balanced strategy between the quality and distribution/quantity of the extracted elevations (Li et al., 2021). Here, based on our previous study, we extracted two types of seed points from the ICESat-2 altimeter data through different combinations of evaluation labels. The first type of seed point (FYSP) was extracted by a comprehensive evaluation label to ensure as high an elevation quality as possible. The second type of seed point (SYSP) were extracted by partial assessment labels (outliers and atmospheric
210   assessments) to ensure good elevation quality and good quantity/distribution. According to the two types of seed points, there are two strategies for the adjustment of the adoption: 1) the adjustment strategy of seed point number (ASSPN); and 2) the adjustment strategy of seed point distribution (ASSPD).

For ASSPN, it was necessary to consider two situations for each $1° \times 1°$ DEM: 1) the quantity of ICESat-2 altimeter data increases with the increase of latitude; and 2) the effective land area is different at the same latitude. To this end, the type of
215   seed point to adopt was related to the maximum latitude Φ_m^{max} and effective land proportion of the modeling area r_{land}, as shown in the following equations. If the number of FYSP is higher than N_S, FYSP was adopted; otherwise, SYSP was adopted.

$$N_S = r_{land} \cdot cos(\Phi_m^{max}) \cdot N_o \tag{11}$$

$$r_{land} = \frac{|P_m^{nw}|}{|P_m|} \tag{12}$$

ASSPD can be expected to obtain a better spatial distribution of seed points and is a supplement for ASSPN. ASSPD is used
220   for a situation in which ASSPN adopts FYSP as SYSP has a good quantity/distribution. ASSPD quantifies the distribution of the first type of seed point by dividing each modeling area into sub-regions and then uses the second type of seed point to

replace the regions with a low number of seed points. As shown in the following formulas, each modeling area was evenly divided into sub-regions (30 × 30 was adopted in this study) to generate a set P_I that a statistic results of the number of the seed points in each sub-region.

$$P_I = \bigcup_{i=1}^{n_I} (\Gamma_i) \tag{13}$$

$$\Gamma_i = \sum_{j=1}^{n} \left\| \frac{\gamma_j^i}{\|\gamma_j^i\|} \right\| \tag{14}$$

$$\gamma_j^i = \tau_j \left(\lambda_j \in [\Lambda_i^{min}, \Lambda_i^{max}), \varphi_j \in [\Phi_i^{min}, \Phi_i^{max}) \right) \tag{15}$$

$$\Lambda_i^{min} = \Lambda_m^{min} + (i-1) \cdot \frac{\Lambda_m^{max} - \Lambda_m^{min}}{\sqrt{n_I}} \tag{16}$$

$$\Lambda_i^{max} = \Lambda_m^{min} + i \cdot \frac{\Lambda_m^{max} - \Lambda_m^{min}}{\sqrt{n_I}} \tag{17}$$

$$\Phi_i^{min} = \Phi_m^{min} + (i-1) \cdot \frac{\Phi_m^{max} - \Phi_m^{min}}{\sqrt{n_I}} \tag{18}$$

$$\Phi_i^{max} = \Phi_m^{min} + i \cdot \frac{\Phi_m^{max} - \Phi_m^{min}}{\sqrt{n_I}} \tag{19}$$

After obtaining P_I, the median N_{median} (except for zeros, thus reducing the influence of the blank regions of seed points) was calculated. The parts P_{add} from which the number of seed points was less than half of N_{median} were then identified, as shown below. Finally, in the sub-regions belonging to P_{add}, SYSP was replaced with FYSP.

$$N_{median} = M\left(P_I(\Gamma_i \neq 0, i = 1,2 \dots N_I) \right) \tag{20}$$

$$P_{add} \in \left\{ P_I < \frac{N_{median}}{2} \right\} \tag{21}$$

where $M(\cdot)$ represents the median calculation.

Finally, all of the collected seed points matched the ASTER GDEM elevations within the modeling area, based on the criterion of the nearest geographical location, and the matched elevations were used to obtain the elevation deviations of the ASTER GDEM.

3.4. GDEM Elevation Correction

For each DEM file of the ASTER GDEM, a random forest regression algorithm was used to train its elevation correction model. The random forest regression function (fitrensemble) of the MATLAB platform was directly used for its processing efficiency and compatibility, and its recommended/default setting values (including the number of trees was 100, etc.) were adopted. Moreover, the training model had a minimum requirement for the seed points' number within the modeling area. If

this number was less than 100, it was necessary to expand the modeling area by adjusting k, as shown in the following formula, and then repeat from part A in Figure 3, i.e., "DEM Prepossessing".

$$k = min(\{0.1, 0.2, \dots 1\}, L + 2 \cdot (L - \Delta L)) \tag{22}$$

After obtaining the model, all the DEM elevations were corrected by the model, and then a new DEM file was generated with
250 the same format.

4. Results and Discussion

4.1. Release of the Corrected ASTER DEM Product

Based on the presented scheme, we corrected the ASTER GDEM elevation with ICESat-2 altimeter data and then stored the corrected ASTER GDEM product (IC2-GDEM) in the GeoTIFF format (.tif) with the same projection and datum as the ASTER
255 GDEM (Xie et al., 2024). The IC2-GDEM product has been openly released via the National Tibetan Plateau Data Center (DOI: 10.11888/RemoteSen.tpdc.301229).
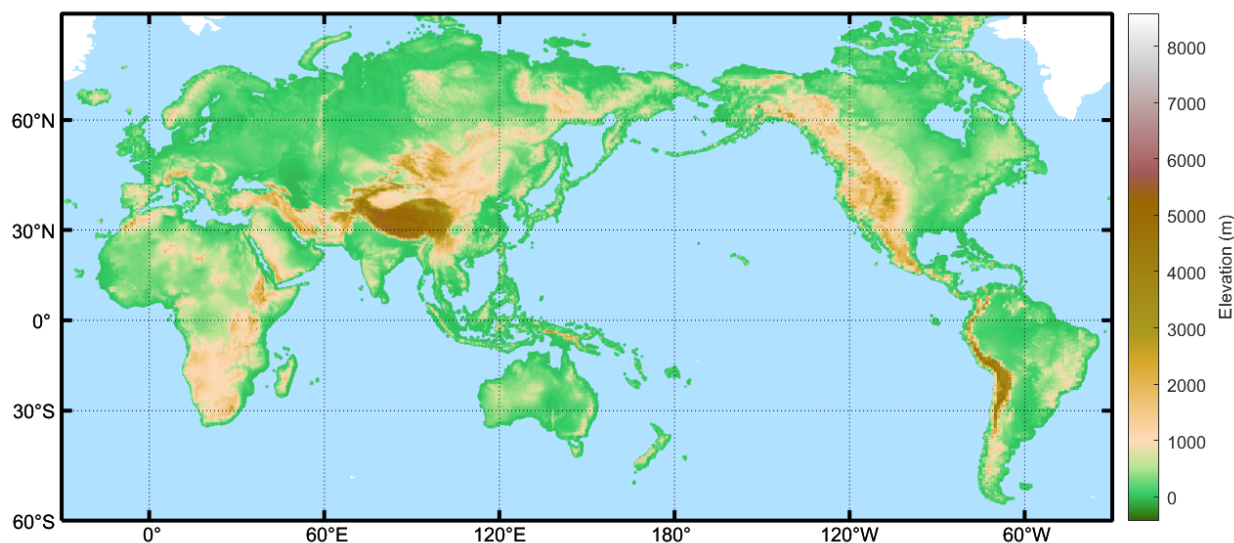
Figure 4: ASTER GDEM product after ICESat-2 altimeter data correction.

Figure 4 shows the distribution of the IC2-GDEM product. IC2-GDEM covers the global land area between 83°N and 60°S,
260 except for the polar regions. Under this coverage, approximately 99.98% of the ASTER GDEM elevation has been corrected, and the remaining ASTER GDEM elevation has not been corrected mainly because of the lack of sufficient ICESat-2 seed points, i.e. the ICESat-2 seed points did not satisfy the constraints of the presented methodology. The uncorrected ASTER GDEM elevation areas are mainly parts of islands and reefs where the geolocation is near low-latitude regions.

4.2. Validation by the High-quality Elevation Control Point Dataset at a Global Scale

265   By using the HAGECPD data, we validated and then contrasted the accuracy of the original and corrected ASTER GDEM elevation within various continents, including Asia, Africa, South America, Oceania, North America, and Europe. Figure 5 provides the statistic results.

The results from the comparison indicate that the accuracy of the corrected ASTER GDEM elevation is higher than that of the original GDEM elevation. In the different continents, the RMSEs of the corrected ASTER GDEM elevation are about 2 to

270   4.5 m, and those of the original ASTER GDEM elevation are about 8 to 10 m. After the elevation correction, the errors of the ASTER GDEM elevation are reduced by more than 45%, and the maximum reduction ratio exceeds 70%. Moreover, there is an obvious difference in the corrected ASTER GDEM elevation errors for the different continents. The elevation error for the continents in order from lowest to highest is: Oceania, South America, Africa, North America, Asia, and Europe. The order of the original ASTER GDEM elevation errors is similar to the above order. To further evaluate the correction performance for

275   the various geolocations, we scrutinized the accuracy of the original and corrected ASTER GDEM elevations in different longitude and latitude regions. Results from the scrutiny are displayed in Figure 6 and Figure 7.
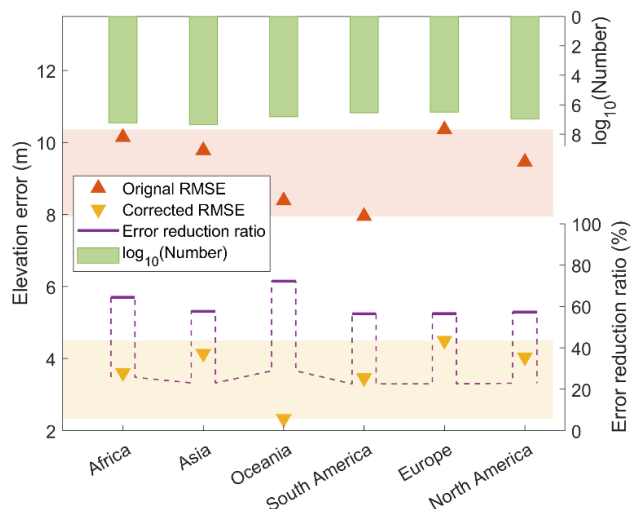
Figure 5: Comparison of the accuracy of the original and corrected ASTER GDEM elevation within different continents.

From Figure 6, in the different longitude regions, it is apparent that, compared with the original ASTER GDEM elevation, the

280   systematic error and standard deviation after ASTER GDEM elevation correction are significantly reduced. In particular, for the original ASTER GDEM elevation, there is a large difference in the systematic error. The systematic error of the original ASTER GDEM elevation in the low-longitude regions is smaller than that in the high-longitude regions. The systematic error after ASTER GDEM elevation correction is close to zero in the different longitude regions.

Similar to the analysis results in Figure 6, in the different latitude regions, it is also apparent that the systematic error and

285   standard deviation after ASTER GDEM elevation correction are significantly reduced, compared with the original ASTER GDEM elevation, as displayed in Figure 7. Notably, the data density of the ICESat-2 laser altimeter data varies greatly in

different latitude regions, and the data density of the ICESat-2 laser altimeter data in the low-latitude regions is generally less than that in the high-latitude regions (Neuenschwander and Pitts, 2019; Markus et al., 2017). However, the errors of the ASTER GDEM elevation corrections in low-latitude regions (especially near the equator) are no larger than those in other latitude
290 regions, which indicates that the correction results are less affected by the difference in the data density of the ICESat-2 laser altimeter data. Moreover, the errors of the ASTER GDEM elevation corrections are larger in high-latitude regions, especially in the Northern Hemisphere. The primary cause for this phenomenon is that the original ASTER GDEM elevation errors in the high-latitude regions are significantly larger than those in other regions.
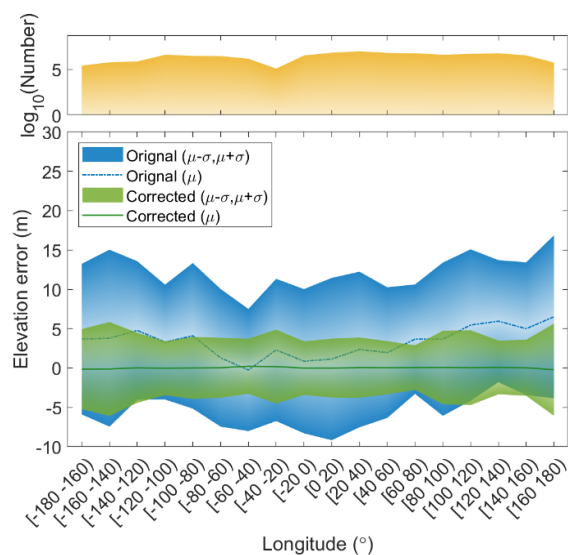
295 **Figure 6: Comparison of the error of the original and corrected ASTER GDEM elevation within different longitude regions.**
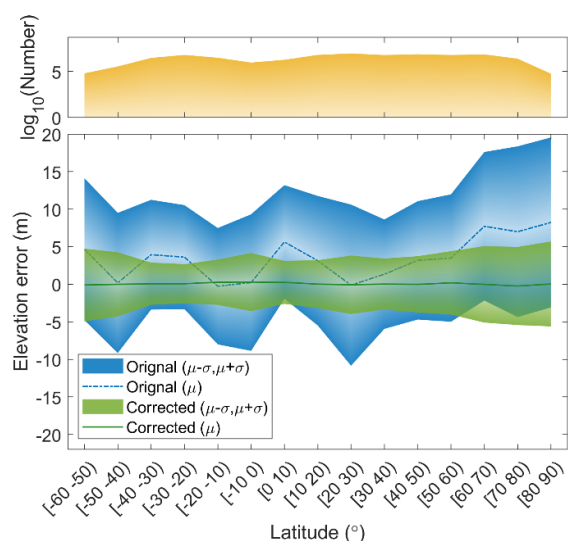
Figure 7: Comparison of the error of the original and corrected ASTER GDEM elevation within different latitude regions.

4.3. Validation by LDEM

By using the LDEM data from around the world (as shown in Figure 2), we validated the errors of the ASTER GDEM elevation
300   before and after correction and then qualified the error reduction ratio of the corrected ASTER GDEM elevation. Table 2
displays the results.

Table 2 Comparison of the error of the original and corrected ASTER GDEM elevation in the different LDEM areas

Area	Original RMSE (m)	Corrected RMSE (m)	Error reduction ratio (%)
a	10.69	3.71	65.33
b	7.01	3.04	56.68
c	9.33	1.63	82.49
d	10.73	3.53	67.14
e	7.27	3.44	52.74
f	11.68	6.33	45.82
g	8.46	4.34	48.73
h	7.63	5.16	32.38
i	11.09	7.44	32.95
j	5.46	1.83	66.51
k	3.82	3.15	17.55
l	7.22	4.57	36.78
m	19.37	12.51	35.42
n	7.97	4.26	46.53
o	7.71	6.47	16.14
p	11.81	4.36	63.04
q	5.68	3.54	37.71
r	5.98	1.88	68.57
s	9.56	5.81	39.26
t	11.50	5.15	55.23
u	12.56	7.19	42.79
v	13.21	9.99	24.39
w	8.56	2.14	75.04
All	9.38	3.37	64.05

From Table 2, it can be seen that the errors of the ASTER GDEM elevation after correction are significantly reduced. For all
305   of the validation areas, the average RMSE of the original ASTER GDEM is 9.38 m, that of the corrected ASTER GDEM is
3.37 m, and the reduction ratio of the elevation error of the corrected ASTER GDEM is 64.05% when compared with the
original ASTER GDEM. For the individual validation areas, the RMSEs of the original ASTER GDEM are between 3.82 and
19.37 m, and those of the corrected ASTER GDEM are between 1.63 and 12.51 m. Compared with the original ASTER GDEM,
the reduction ratio of the elevation error of the corrected ASTER GDEM ranges from 16.14% to 82.49%, corresponding to an
310   average of 47.66%.

Figure 8 provides a more detailed evaluation of the error distribution of the original and corrected ASTER GDEM elevation.
In each plane, the red and orange histograms represent the error distribution of the original and corrected ASTER GDEM,
respectively. From Figure 8, it can be seen that the error distributions of the corrected ASTER GDEM elevation show better
symmetry at zero error than those of the original ASTER GDEM elevation. This phenomenon indicates that the systematic
315   error of the original ASTER GDEM elevation has been well corrected. Meanwhile, the statistical dispersion of the error
distribution of the corrected ASTER GDEM elevation is significantly smaller than that of the original ASTER GDEM elevation.
Moreover, there are differences between these statistical descriptions. This phenomenon is mainly caused by differences in
topography and the Earth's surface. To confirm this, we combined other data, including LDEM data, vegetation cover index
data (GFCC30TC), and land-cover data (FROM-GLC10), to evaluate the influence of these two factors. Results from the
320   analysis are provided in Figure 9 and Figure 10. For terrain, we used the commonly used topographic indicator—slope—to
quantify the topographic relief. The slope was obtained through ArcGIS processing. After the slope was obtained, we first
divided it into different slope intervals and then calculated the errors after ASTER GDEM elevation correction in each interval.
Meanwhile, the errors of the original ASTER GDEM elevation were added to the statistical analysis to further supplement the
investigation of the correction results. To examine the different surfaces of Earth, we first divided it into urban, bare land, and
325   vegetation areas, according to the land-cover data, and then carried out statistical analysis of the errors of the original and
corrected ASTER GDEM elevation in each area. We then carried out subdivision and statistical analysis of the vegetation
areas through the vegetation cover data.
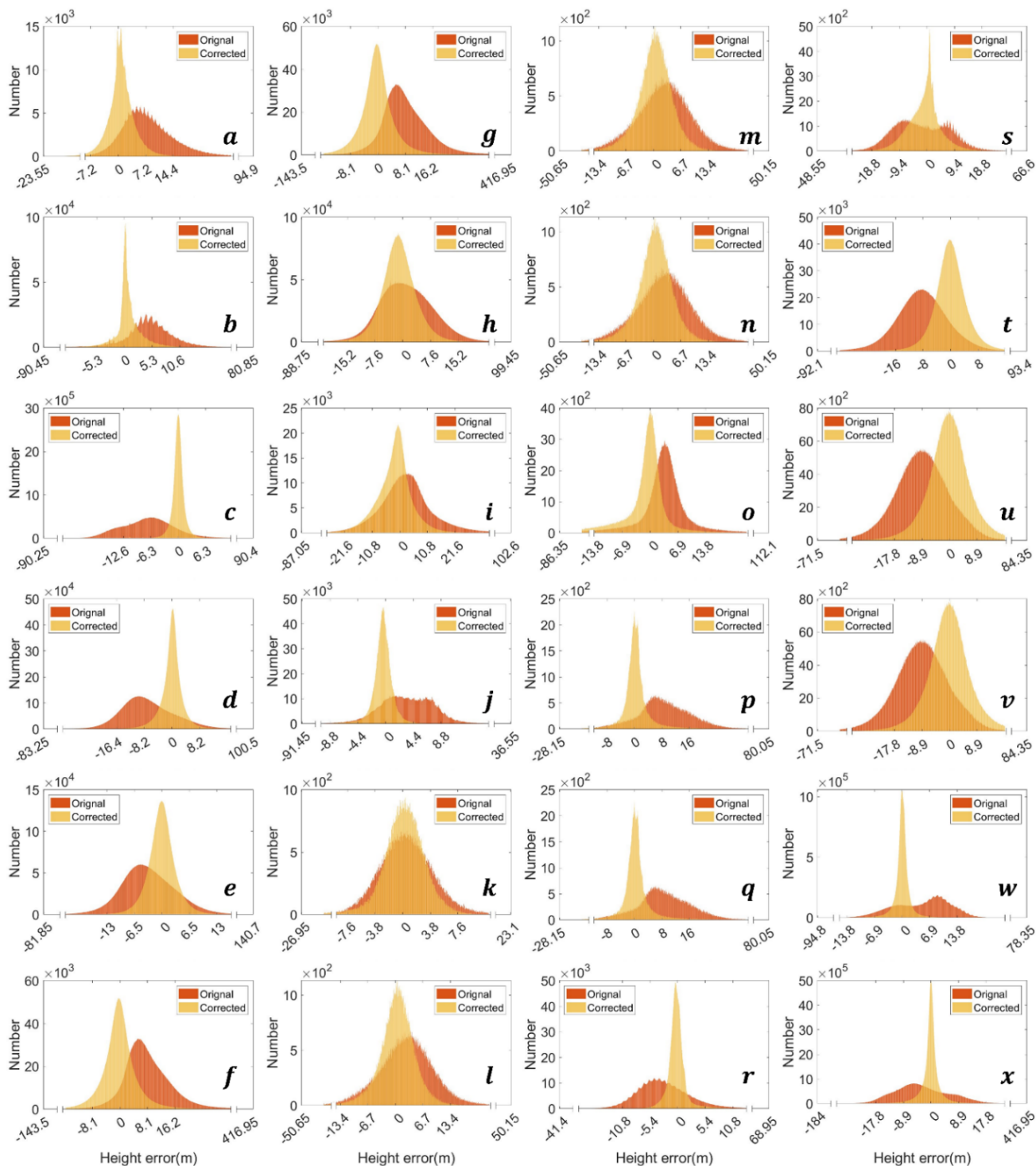
Figure 8: Comparison of the original and corrected ASTER GDEM elevation error.

330
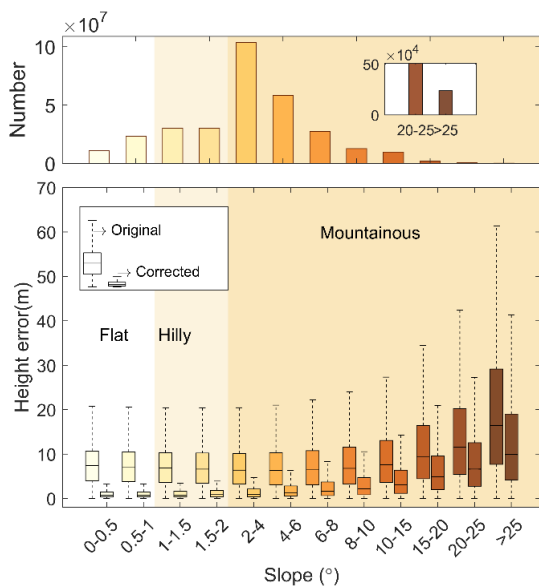
Figure 9: Comparison of the original and corrected ASTER GDEM elevation error with different slopes.
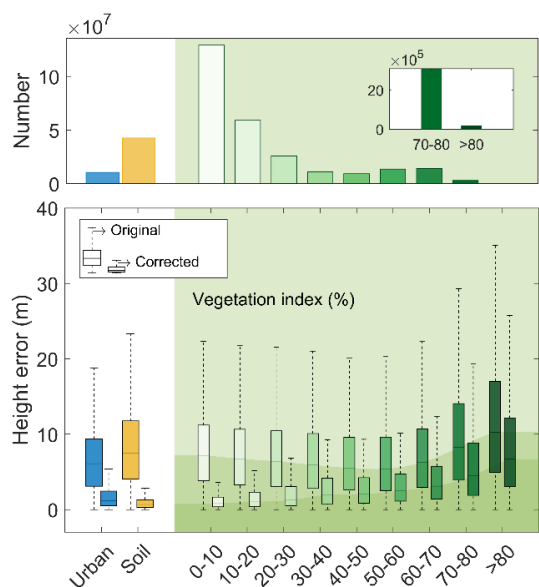
Figure 10: Comparison of the original and corrected ASTER GDEM elevation error with different land covers.

335 From Figure 9, it is apparent that, in the different slope regions, the errors of the corrected GDEM elevation are significantly reduced when compared with those of the original GDEM elevation, which indicates that the corrected results have a better elevation quality in the areas with different topographic relief. Meanwhile, this kind of error decrease shows a weakening trend with the increase of the slope. There are two main reasons for this trend. The first reason is that the quality of data from the

ICESat-2 laser altimeter, which were used as the seed points, generally decreases as the slope increases. The second reason is
340   that the accuracy of the original ASTER GDEM elevation also decreases as the slope increases, as shown in Figure 9.

From Figure 10, under the three different Earth surface categories, it can be seen that the errors of the corrected GDEM elevation are all significantly smaller than those of the original GDEM elevation. For the different land covers, the corrected GDEM elevation in the bare land areas shows the best elevation correction. Compared with the other two types of ground objects, the bare land area is not shielded by ground objects, which is conducive to optical observation of ground texture (Li
345   et al., 2023a; Pham et al., 2018) and laser detection of ground elevation (Li et al., 2023b; Neuenschwander and Pitts, 2019). Therefore, there is little need to consider the influence of ground objects on terrain elevation in bare land areas. For the other two types of land cover, the corrected GDEM elevation quality in the areas with low vegetation cover (less than 20% vegetation cover index) is comparable to that in the urban areas, but with the increase of vegetation cover, the difference in the corrected GDEM elevation quality between the two types of land cover gradually increases. Moreover, relative to the original GDEM
350   elevation, the quality improvement of the corrected GDEM elevation shows a reduced trend with the increase in vegetation cover. Similar to the analysis of topographic relief, there are two main reasons for this phenomenon, i.e., the quality of the ICESat-2 laser altimeter data and the accuracy of the original ASTER GDEM elevation both decrease as the vegetation cover increases.

From the above analysis, while the IC2-GDEM demonstrates significant improvements in elevation accuracy, its quality of
355   elevation correction is notably limited in the areas with steep slopes or high vegetation cover index. For research or applications with high-quality elevation requirements, this limitation can be quantified and identified through topographic relief calculations or in combination with vegetation cover data. Moreover, the temporal differences between the ICESat-2 data survey and ASTER GDEM collection may lead to elevation inconsistencies, especially in extremely dynamic landscapes (e.g., coastal erosion areas). Integrating IC2-GDEM with other elevation data (closer to the ASTER GDEM data collection time)
360   can weaken the impact of the inconsistencies and reduce deviations of the analysis results in this kind of landscape.

5. Conclusion

In this study, we introduce a new open-source dataset, named IC2-GDEM. IC2-GDEM is generated by directly refining the ASTER GDEM elevation with ICESat-2 altimeter data, as well as FROM-GLC10 data and GFCC30TC data. This strategy leverages existing datasets and enhances them with additional data and it is cost-effective for improving elevation accuracy,
365   which is particularly beneficial for applications in developing regions where resources to obtain high-accuracy DEMs may be limited.

The elevation quality of IC2-GDEM has been evaluated at a global scale and in multiple local regions by using other laser/LiDAR data from satellite or airborne platforms. From the evaluation results for the different geolocations at a global scale, it was found that the correction results are less affected by the difference in the data density of the ICESat-2 laser
370   altimeter data. ICESat-2 observations at higher-latitude areas are denser than those at lower-latitude areas. However, the errors

of the IC2-GDEM elevation in low-latitude regions are no larger than the errors in high-latitude regions. From the evaluation results for the different topographies, the ASTER GDEM after elevation correction shows an obvious improvement of elevation quality for the different topographies, even in the mountainous areas with higher slopes. A similar conclusion was also found from the evaluation of the different land covers. These analysis results show that the IC2-GDEM presents a superior elevation quality at a global scale.

IC2-GDEM is expected to promote seamless integration with the historical datasets of ASTER GDEM, which is essential for longitudinal studies of long-term environmental changes, land use dynamics, and climate impacts. As a dataset for exploring the quality improvement of GDEM sourced from optical imaging, IC2-GDEM can serve as a new complementary data source for other GDEMs, such as SRTM, and Copernicus DEM. Researchers can combine IC2-GDEM with other DEMs to cross-validate qualities, fill data gaps, and conduct multi-scale analyses for earth science studies such as Flood risk, climate change, etc. with more reliable and comprehensive scientific discoveries.

References

Abrams, M., Crippen, R., and Fujisada, H.: ASTER Global Digital Elevation Model (GDEM) and ASTER Global Water Body Dataset (ASTWBD), doi:10.3390/rs12071156, 2020.

Abrams, M., Tsu, H., Hulley, G., Iwao, K., Pieri, D., Cudahy, T., and Kargel, J.: The Advanced Spaceborne Thermal Emission and Reflection Radiometer (ASTER) after fifteen years: Review of global products, Int. J. Appl. Earth Obs. Geoinf., 38, 292-301, doi:10.1016/j.jag.2015.01.013, 2015.

Al-Areeq, A. M., Sharif, H. O., Abba, S. I., Chowdhury, S., Al-Suwaiyan, M., Benaafi, M., Yassin, M. A., and Aljundi, I. H.: Digital elevation model for flood hazards analysis in complex terrain: Case study from Jeddah, Saudi Arabia, Int. J. Appl. Earth Obs. Geoinf., 119, 103330, doi:10.1016/j.jag.2023.103330, 2023.

Ao, Z., Hu, X., Tao, S., Hu, X., Wang, G., Li, M., Wang, F., Hu, L., Liang, X., Xiao, J., Yusup, A., Qi, W., Ran, Q., Fang, J., Chang, J., Zeng, Z., Fu, Y., Xue, B., Wang, P., Zhao, K., Li, L., Li, W., Li, Y., Jiang, M., Yang, Y., Shen, H., Zhao, X., Shi, Y., Wu, B., Yan, Z., Wang, M., Su, Y., Hu, T., Ma, Q., Bai, H., Wang, L., Yang, Z., Feng, Y., Zhang, D., Huang, E., Pan, J., Ye, H., Yang, C., Qin, Y., He, C., Guo, Y., Cheng, K., Ren, Y., Yang, H., Zheng, C., Zhu, J., Wang, S., Ji, C., Zhu, B., Liu, H., Tang, Z., Wang, Z., Zhao, S., Tang, Y., Xing, H., Guo, Q., Liu, Y., and Fang, J.: A national-scale assessment of land subsidence in China's major cities, Science, 384, 301-306, doi:10.1126/science.adl4366, 2024.

Cook, A. J., Murray, T., Luckman, A., Vaughan, D. G., and Barrand, N. E.: A new 100-m Digital Elevation Model of the Antarctic Peninsula derived from ASTER Global DEM: methods and accuracy assessment, Earth Syst. Sci. Data, 4, 129-142, doi:10.5194/essd-4-129-2012, 2012.

Crippen, R., Buckley, S., Agram, P., Belz, E., Gurrola, E., Hensley, S., Kobrick, M., Lavalle, M., Martin, J., Neumann, M., Nguyen, Q., Rosen, P., Shimada, J., Simard, M., and Tung, W.: NASADEM GLOBAL ELEVATION MODEL: METHODS

AND PROGRESS, ISPRS - International Archives of the Photogrammetry, Remote Sensing and Spatial Information Sciences, XLI-B4, 125-128, doi:10.5194/isprs-archives-XLI-B4-125-2016, 2016.

del Rosario González-Moradas, M., Viveen, W., Andrés Vidal-Villalobos, R., and Carlos Villegas-Lanza, J.: A performance comparison of SRTM v. 3.0, AW3D30, ASTER GDEM3, Copernicus and TanDEM-X for tectonogeomorphic analysis in the South American Andes, CATENA, 228, 107160, doi:10.1016/j.catena.2023.107160, 2023.

Dubayah, R., Blair, J. B., Goetz, S., Fatoyinbo, L., Hansen, M., Healey, S., Hofton, M., Hurtt, G., Kellner, J., Luthcke, S., Armston, J., Tang, H., Duncanson, L., Hancock, S., Jantz, P., Marselis, S., Patterson, P. L., Qi, W., and Silva, C.: The Global Ecosystem Dynamics Investigation: High-resolution laser ranging of the Earth's forests and topography, Sci. Remote Sens., 1, 100002, doi:10.1016/j.srs.2020.100002, 2020.

Fahrland, E., Paschko, H., Jacob, P., and Kahabka, H.: Copernicus DEM Product Handbook, Airbus Defense and Space GmbH, AlemaniaAO/1-9422/18/I-LG, 2022.

Fan, Y., Ke, C.-Q., and Shen, X.: A new Greenland digital elevation model derived from ICESat-2, 10.5194/essd-2021-183, 2021.

Fan, Y., Ke, C. Q., and Shen, X.: A new Greenland digital elevation model derived from ICESat-2 during 2018–2019, Earth Syst. Sci. Data, 14, 781-794, doi:10.5194/essd-14-781-2022, 2022.

Farr, T. G., Rosen, P. A., Caro, E., Crippen, R., Duren, R., Hensley, S., Kobrick, M., Paller, M., Rodriguez, E., Roth, L., Seal, D., Shaffer, S., Shimada, J., Umland, J., Werner, M., Oskin, M., Burbank, D., and Alsdorf, D.: The Shuttle Radar Topography Mission, Rev. Geophys., 45, doi:10.1029/2005RG000183, 2007.

Fernandez-Diaz, J. C., Velikova, M., and Glennie, C. L.: Validation of ICESat-2 ATL08 Terrain and Canopy Height Retrievals in Tropical Mesoamerican Forests, IEEE J. Sel. Top. Appl. Earth Obs. Remote Sens., 15, 2956-2970, doi:10.1109/JSTARS.2022.3163208, 2022.

Franks, S., Storey, J., and Rengarajan, R.: The New Landsat Collection-2 Digital Elevation Model, doi:10.3390/rs12233909, 2020.

García-Álvarez, D. and Lara Hinojosa, J.: Global Thematic Land Use Cover Datasets Characterizing Vegetation Covers, in: Land Use Cover Datasets and Validation Tools: Validation Practices with QGIS, edited by: García-Álvarez, D., Camacho Olmedo, M. T., Paegelow, M., and Mas, J. F., Springer International Publishing, Cham, 373-398, doi:10.1007/978-3-030-90998-7_19, 2022.

Gong, P., Liu, H., Zhang, M., Li, C., Wang, J., Huang, H., Clinton, N., Ji, L., Li, W., Bai, Y., Chen, B., Xu, B., Zhu, Z., Yuan, C., Suen, H., Guo, J., Xu, N., Li, W., Zhao, Y., and Song, L.: Stable classification with limited sample: transferring a 30-m resolution sample set collected in 2015 to mapping 10-m resolution global land cover in 2017, Sci. Bull., 64, doi:10.1016/j.scib.2019.03.002, 2019.

Hawker, L., Neal, J., and Bates, P.: Accuracy assessment of the TanDEM-X 90 Digital Elevation Model for selected floodplain sites, Remote Sens. Environ., 232, 111319, doi:10.1016/j.rse.2019.111319, 2019.

435 Hawker, L., Uhe, P., Paulo, L., Sosa, J., Savage, J., Sampson, C., and Neal, J.: A 30 m global map of elevation with forests and buildings removed, Environ. Res. Lett., 17, 024016, doi:10.1088/1748-9326/ac4d4f, 2022.

Huang, J. and Yu, Y.: Vertical Accuracy Assessment of the ASTER, SRTM, GLO-30, and ATLAS in a Forested Environment, doi:10.3390/f15030426, 2024.

Li, B., Xie, H., Tong, X., Tang, H., and Liu, S.: A Global-Scale DEM Elevation Correction Model Using ICESat-2 Laser
440 Altimetry Data, IEEE Trans. Geosci. Remote Sens., 61, 1-15, doi:10.1109/TGRS.2023.3321956, 2023a.

Li, B., Xie, H., Liu, S., Sun, Y., Xu, Q., and Tong, X.: Correction of ICESat-2 terrain within urban areas using a water pump deployment criterion with the vertical contour of the terrain, Remote Sens. Environ., 298, 113817, doi:10.1016/j.rse.2023.113817, 2023b.

Li, B., Xie, H., Tong, X., Liu, S., Xu, Q., and Sun, Y.: Extracting accurate terrain in vegetated areas from ICESat-2 data, Int.
445 J. Appl. Earth Obs. Geoinf., 117, 103200, doi:10.1016/j.jag.2023.103200, 2023c.

Li, B., Xie, H., Tong, X., Tang, H., Liu, S., Jin, Y., Wang, C., and Ye, Z.: High-Accuracy Laser Altimetry Global Elevation Control Point Dataset for Satellite Topographic Mapping, IEEE Trans. Geosci. Remote Sens., 60, 1-1, doi:10.1109/TGRS.2022.3177026, 2022.

Li, B. B., Xie, H., Liu, S. J., Tong, X. H., Tang, H., and Wang, X.: A Method of Extracting High-Accuracy Elevation Control
450 Points from ICESat-2 Altimetry Data, Photogramm. Eng. Remote Sens., 87, 821-830, doi:10.14358/PERS.21-00009R2, 2021.

Li, P., Shi, C., Li, Z., Muller, J.-P., Drummond, J., Li, X., Li, T., Li, Y., and Liu, J.: Evaluation of ASTER GDEM using GPS benchmarks and SRTM in China, Int. J. Remote Sens., 34, 1744-1771, doi:10.1080/01431161.2012.726752, 2013.

Magruder, L., Neuenschwander, A., and Klotz, B.: Digital terrain model elevation corrections using space-based imagery and ICESat-2 laser altimetry, Remote Sens. Environ., 264, 112621, doi:10.1016/j.rse.2021.112621, 2021.

455 Markus, T., Neumann, T., Martino, A., Abdalati, W., Brunt, K., Csatho, B., Farrell, S., Fricker, H., Gardner, A., Harding, D., Jasinski, M., Kwok, R., Magruder, L., Lubin, D., Luthcke, S., Morison, J., Nelson, R., Neuenschwander, A., Palm, S., Popescu, S., Shum, C. K., Schutz, B. E., Smith, B., Yang, Y. K., and Zwally, J.: The Ice, Cloud, and land Elevation Satellite-2 (ICESat-2): Science requirements, concept, and implementation, Remote Sens. Environ., 190, 260-273, doi:10.1016/j.rse.2016.12.029, 2017.

460 Martino, A. J., Neumann, T., Kurtz, N., and McLennan, D.: ICESat-2 mission overview and early performance, 2019/10/10, doi:10.1117/12.2534938, 2019.

Meadows, M., Jones, S., and Reinke, K.: Vertical accuracy assessment of freely available global DEMs (FABDEM, Copernicus DEM, NASADEM, AW3D30 and SRTM) in flood-prone environments, Int. J. Digital Earth, 17, 2308734, doi:10.1080/17538947.2024.2308734, 2024.

465 Neuenschwander, A. and Pitts, K.: The ATL08 land and vegetation product for the ICESat-2 Mission, Remote Sens. Environ., 221, 247-259, doi:10.1016/j.rse.2018.11.005, 2019.

Neuenschwander, A., Guenther, E., White, J. C., Duncanson, L., and Montesano, P.: Validation of ICESat-2 terrain and canopy heights in boreal forests, Remote Sens. Environ., 251, doi:10.1016/j.rse.2020.112110, 2020.

Okolie, C. J. and Smit, J. L.: A systematic review and meta-analysis of Digital elevation model (DEM) fusion: pre-processing,
470   methods and applications, ISPRS J. Photogramm. Remote Sens., 188, 1-29, doi:10.1016/j.isprsjprs.2022.03.016, 2022.

Okolie, C. J., Mills, J. P., Adeleke, A. K., Smit, J. L., Peppa, M. V., Altunel, A. O., and Arungwa, I. D.: Assessment of the
global Copernicus, NASADEM, ASTER and AW3D digital elevation models in Central and Southern Africa, Geo-spatial Inf.
Sci., 1-29, doi:10.1080/10095020.2023.2296010, 2024.

Pham, H. T., Marshall, L., Johnson, F., and Sharma, A.: A method for combining SRTM DEM and ASTER GDEM2 to improve
475   topography estimation in regions without reference data, Remote Sens. Environ., 210, 229-241, doi:10.1016/j.rse.2018.03.026,
2018.

Schutz, B., Zwally, H., Shuman, C. A., and Hancock, D.: Overview of the ICESat mission, Geophys. Res. Lett., 32,
doi:10.1029/2005GL02400, 2005.

Sexton, J. O., Song, X.-P., Feng, M., Noojipady, P., Anand, A., Huang, C., Kim, D.-H., Collins, K. M., Channan, S., DiMiceli,
480   C., and Townshend, J. R.: Global, 30-m resolution continuous fields of tree cover: Landsat-based rescaling of MODIS
vegetation continuous fields with lidar-based estimates of error, Int. J. Digital Earth, 6, 427-448,
doi:10.1080/17538947.2013.786146, 2013.

Shen, X., Ke, C.-Q., Fan, Y., and Drolma, L.: A new digital elevation model (DEM) dataset of the entire Antarctic continent
derived from ICESat-2, Earth Syst. Sci. Data, 14, 3075-3089, doi:10.5194/essd-14-3075-2022, 2022.

485   Tang, X., Xie, J., Liu, R., Huang, G., Zhao, C., Zhen, Y., Tang, H., and Dou, X.: Overview of the GF‑7 Laser Altimeter
System Mission, Earth Space Sci., 7, doi:10.1029/2019EA000777, 2020.

Xie, H., Li, B., Liu, S., Ye, Z., Hong, Z., Sun, Y., Xu, Q., and Tong, X.: ICESat-2 corrected GDEM product (IC2-GDEM):
Global digital elevation model refined by ICESat-2 laser altimeter data corrections to the ASTER GDEM, National Tibetan
Plateau Data Center [dataset], doi:10.11888/RemoteSen.tpdc.301229, 2024.

490   Xie, H., Li, B., Tong, X., Zhang, X., He, T., Dai, J., Huang, G., Zhang, Z., and Liu, S.: A Planimetric Location Method for
Laser Footprints of the Chinese Gaofen-7 Satellite Using Laser Spot Center Detection and Image Matching to Stereo Image
Product, IEEE Trans. Geosci. Remote Sens., PP, 1-14, doi:10.1109/TGRS.2020.3048042, 2021.

Yamazaki, D., Ikeshima, D., Tawatari, R., Yamaguchi, T., O'Loughlin, F., Neal, J. C., Sampson, C. C., Kanae, S., and Bates,
P. D.: A high-accuracy map of global terrain elevations, Geophys. Res. Lett., 44, 5844-5853, doi:10.1002/2017GL072874,
495   2017.

Yue, L., Shen, H., Zhang, L., Zheng, X., Zhang, F., and Yuan, Q.: High-quality seamless DEM generation blending SRTM-1,
ASTER GDEM v2 and ICESat/GLAS observations, ISPRS J. Photogramm. Remote Sens., 123, 20-34,
doi:10.1016/j.isprsjprs.2016.11.002, 2017.

Zhu, J., Yang, P.-f., Li, Y., Xie, Y.-z., and Fu, H.-q.: Accuracy assessment of ICESat-2 ATL08 terrain estimates: A case study
500   in Spain, J. Cent. South Univ., 29, 226-238, doi:10.1007/s11771-022-4896-x, 2022.

Data availability

All the data used in this study are open source. The IC2-GDEM is available via https://doi.org/10.11888/RemoteSen.tpdc.301229 (Xie et al., 2024). The ICESat-2 ATL08 product is available via
505 https://lpdaac.usgs.gov/. The ASTER GDEM product is available via https://lpdaac.usgs.gov/. The global land-cover data (FROM-GLC10) are available via http://data.ess.tsinghua.edu.cn/fromglc10_2017v01.html. The vegetation cover index data (GFCC30TC v003) are available via https://lpdaac.usgs.gov/products/gfcc30tcv003/. The HAGECPD data are available via 10.11888/Geogra.tpdc.271727. The high-resolution and accurate LDEM data are available via https://data.linz.govt.nz/, https://www.noaa.gov/, https://www.ahn.nl/, https://www.ign.gob.ar/, and https://ecat.ga.gov.au/.

510 **Funding**

This research was supported by the National Natural Science Foundation of China (grant no. 42325106, 42221002), the Shanghai Academic Research Leader Program (grant no. 23XD1404100), and the Fundamental Research Funds for the Central Universities of China.

Author contributions

515 Binbin Li: Writing – original draft, Visualization, Methodology. Huan Xie: Conceptualization, Writing – review & editing, Funding acquisition. Shijie Liu: Investigation, Resources. Zhen Ye: Investigation, Resources. Zhonghua Hong: Investigation. Qihao Weng: Investigation. Yuan Sun: Data curation, Validation. Qi Xu: Software, Validation. Xiaohua Tong: Funding acquisition, Supervision.

Competing interests

520 The contact author has declared that none of the authors has any competing interests.